arXiv:0812.1312v1 [quant-ph] 6 Dec 2008

Quantum Trajectory Analysis of Two-mode Microlaser operating on Three-Level Atoms

Tarek Ahmed Mokhiemer Elsayed*
Electronics Research Institute, Cairo, Egypt and
Institute of Theoretical Physics, Heidelberg University, Germany

Abdu Alaziz Aljalal†
King Fahd University of Petroleum and Minerals

(Dated: December 6, 2008)

In this paper, we use the Quantum Trajectory Method, a Monte Carlo Simulation applied to quantum systems, to study a microlaser operating on three-level atoms interacting with a two-mode cavity. We are interested in the quantum statistical properties of the cavity field at steady state. It's shown that steady state solution does exist when the detailed balance condition doesn't apply. We highlight the differences between a single mode microlaser and a two-mode microlaser. Special attention is paid to the one-photon trapping state. The second order correlation function $g^{(2)}(\tau)$ of a single mode is studied. We show the effects of the velocity spread of the atoms used to pump the microlaser cavity on the second order correlation function, trapping states and phase transition of the cavity field. We illustrate an interesting effect of the atomic velocity spread on the coherence function when the cavity field of a mono-velocity atomic beam microlaser exhibits anti-bunching.

I. INTRODUCTION

The single atom laser (microlaser) has been used successfully in the last decade as a source of non-classical light [1, 2, 3]. Following the same principles of the single atom maser (micromaser), the microlaser operates by pumping a high finesse optical cavity by a beam of excited atoms. The microlaser we are considering in this paper is different than the single atom laser first operated by McKeever [4] where one and the same atom is used. We use the "microlaser" term in this paper however to describe the experimental setup of the MIT microlaser [1]. Being one of the best systems to study cavity QED effects, the single atom maser/laser has received a lot of interest in the quantum optics community. One interesting type of microlaser utilizes bi-modal cavities pumped by multi-level atoms [5, 6, 7]. A two-mode micromaser pumped by three-level atoms in Λ-configuration has been analyzed analytically by F. L. Kien et. al. in [7]. In the current work we use the Quantum Trajectory Method [8, 9, 10, 11] to analyze the two-mode microlaser operated by pumping a doubly resonant optical cavity by atoms characterized by two lasing transitions and strongly coupled to the cavity. Atoms used to pump the microlaser cavity are produced by an oven and the velocities of the atoms obey a thermal velocity distribution. The atoms then are let to pass through a velocity selector to unify the speeds of the atoms and consequently their interaction times with the cavity. Since the efficiency of the velocity selector is not perfect, atoms passing through the cavity still have a slight velocity variation. Our main target in this paper is to calculate the cavity field coherence function and investigate the effects of the variation of the atoms' velocities on the coherence function and other statistical properties of the cavity field. This paper is divided into five sections. In Sec. II we review the theory of the two-mode microlaser and the coherence function of the field inside the microlaser cavity and elaborate on the interesting one-photon trapping state. In Sec. III we introduce the Quantum Trajectory Method and apply it to the two-mode microlaser and show the results of calculating the coherence function $g^{(2)}(\tau)$ numerically and analytically. In Sec. IV, we show the results of including the variation of the atoms' velocities in the numerical simulation and elucidate its effect on the statistical properties of the microlaser field. We conclude our work in Sec. V and present suggestions for further investigations.

II. THEORY

A schematic diagram of the energy levels of the three-level atoms used to pump the bi-modal microlaser cavity is shown in Fig. 1. In the most general case, each mode has its own angular frequency ω_α, coupling strength with the atom g_α, decay rate γ_α, and mean number of thermal photons $n_{b_\alpha}$where $\alpha = 1, 2$. Although, unlike the micromaser, the mean number of thermal photons for a microlaser is typically zero, we include n_{b1},n_{b2} in this paper for the sake of generality. All the atoms are excited to the higher level $|a\rangle$ before they enter the cavity. Atoms are statistically independent (have random arrival times) and their dwelling time inside the cavity is much shorter than the mean inter-atomic arrival times.

We assume that the detuning between the two mode frequencies is large, compared to the atom-field coupling strengths g_1, g_2, so that each mode interacts only with the respective atomic transition. Since the cavity is sub-

---

*Electronic address: physics.reality@gmail.com
†Electronic address: Aljalal@kfupm.edu.sa

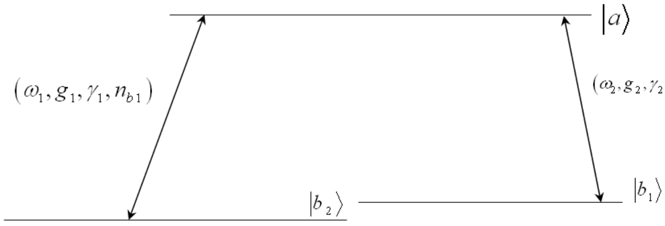
$|a\rangle$
$(\omega_1, g_1, \gamma_1, n_{b1})$
$(\omega_2, g_2, \gamma_2, n_{b2})$
$|b_2\rangle$
$|b_1\rangle$

FIG. 1: A schematic diagram of the energy levels of a three level atom in Λ-configuration

jected to the incoherent field decay, we are going to use density matrix formalism where the field is represented by the density matrix ρ. The diagonal elements of the field density matrix P_{n_1,n_2}, which represent the joint probability to find n_1 photons in mode 1 and n_2 photons in mode 2, constitute a two dimensional matrix. In what follows we are going to summarize the procedure given in [7] to calculate the steady state solution of P_{n_1,n_2}. We are not interested in the off-diagonal elements of the density matrix in the current work. Changes to the density matrix are induced by two different and independent procedures, the atom field interaction and the field dissipation from the cavity. The change to the density matrix due to the interaction between the field and a single atom during the interaction time τ_{int} is represented by the superoperator $F(\tau)$ such as $\rho(t_i + \tau_{\text{int}}) = F(\tau_{\text{int}})\,\rho(t_i)$. The field dissipation is controlled by the Liouvillian superoperator $\hat{L}_0$ given by [12]

$$\dot{\rho} = \hat{L}_0\rho = -\frac{1}{2}\gamma_1\left(n_{b1}+1\right)\left[a_1^\dagger a_1\rho + \rho a_1^\dagger a_1 - 2a_1\rho a_1^\dagger\right] - \frac{1}{2}\gamma_1 n_{b1}\left[a_1 a_1^\dagger\rho + \rho a_1 a_1^\dagger - 2a_1^\dagger\rho a_1\right] \tag{1}$$

where $\left(a_1^\dagger, a_1\right)$ *and* $\left(a_2^\dagger, a_2\right)$ are the field operators of the two modes and n_{b1},n_{b2} are the mean number of thermal photons in the two modes. It can be shown [13] that for the random arrival of atoms, which is a Poisson process, the master equation controlling the change of the density matrix ρ is given by

$$\dot{\rho} = R\left[F(\tau_{\text{int}}) - 1\right]\rho + L_0\rho \tag{2}$$

where R is the rate of the atoms injection. At steady state, we have

$$\dot{\rho} = 0 \tag{3}$$

$$R\left[1 - F(\tau_{\text{int}})\right]\rho = L_0\rho \tag{4}$$

which simply means that, the change per unit time in the field density matrix due to the atom field interaction is exactly compensated by the change due to field dissipation from the cavity. In other words the net change per unit time of the field density matrix is zero. To obtain the form of $F(\tau)$, we start by writing the interaction Hamiltonian of the atom-field system during the interaction assuming that the transition between the two ground levels is forbidden:

$$H_{\text{int}} = \hbar g_1\left(a_1^\dagger\sigma_1 + a_1\sigma_1^\dagger\right) + \hbar g_2\left(a_2^\dagger\sigma_2 + a_2\sigma_2^\dagger\right) \tag{5}$$

The Shrodinger's equation in the interaction picture, governing the evolution of the atom-field wavefunction is

$$i\hbar\frac{\partial\left|\psi\right\rangle}{\partial t} = H_{\text{int}}\left|\psi\right\rangle \tag{6}$$

where $|\psi(t)\rangle$ is generally expressed as:

$$|\psi(t)\rangle = \sum_{n,m} c_{a,n,m}\left|a,n,m\right\rangle + c_{b_1,n,m}\left|b_1,n,m\right\rangle + c_{b_2,n,m}\left|b_2,n,m\right\rangle \tag{7}$$

and n, m are the numbers of photons in mode 1 and mode 2 respectively. Since at the beginning of the interaction, the atom is in its excited state, then

$$|\psi(0)\rangle = \sum_{n,m} c_{a,n,m}\left|a,n,m\right\rangle \tag{8}$$

and hence

$$P_{n,m}(0) = \left|c_{a,n,m}\right|^2 \tag{9}$$

Inserting the expression of $|\psi(t)\rangle$ into the Schrodinger's equation we obtain

$$i\dot{c}_{a,n,m} = g_1\sqrt{n+1}c_{b_1,n+1,m} + g_2\sqrt{m+1}c_{b_1,n,m+1} \tag{10}$$

$$i\dot{c}_{b_1,n,m} = g_1\sqrt{n}c_{a,n-1,m} \tag{11}$$

$$i\dot{c}_{b_2,n,m} = g_2\sqrt{m}c_{a,n,m-1} \tag{12}$$

from which we obtain

$$\ddot{c}_{a,n,m} = -\left[g_1^2\left(n+1\right)+g_2^2\left(m+1\right)\right]c_{a,n,m} \tag{13}$$

By solving (11,12,13) and taking the origin of time to be at $t = 0$ we get

$$c_{a,n,m}(\tau_{\rm int}) = c_{a,n,m}(0)cos\sqrt{g_1^2\left(n+1\right)+g_2^2\left(m+1\right)}\tau_{\rm int} \tag{14}$$

$$c_{b_1,n,m}(\tau_{\rm int}) = c_{a,n-1,m}(0)g_1\sqrt{n}\frac{sin\sqrt{g_1^2\left(n\right)+g_2^2\left(m+1\right)}\tau_{\rm int}}{\sqrt{g_1^2\left(n\right)+g_2^2\left(m+1\right)}} \tag{15}$$

$$c_{b_2,n,m}(\tau_{\rm int}) = c_{a,n,m-1}(0)g_2\sqrt{m}\frac{sin\sqrt{g_1^2\left(n+1\right)+g_2^2\left(m\right)}\tau_{\rm int}}{\sqrt{g_1^2\left(n+1\right)+g_2^2\left(m\right)}} \tag{16}$$

Defining

$$\lambda\left(n,m\right) = \sqrt{g_1^2\left(n+1\right)+g_2^2\left(m+1\right)} \tag{17}$$

we conclude that

$$P_{n,m}(\tau_{\rm int}) = P_{n,m}(0)cos^2\left[\lambda\left(n,m\right)\tau_{\rm int}\right] + g_1 n P_{n-1,m}(0)\frac{\sin^2\left[\lambda\left(n-1,m\right)\tau_{\rm int}\right]}{\lambda^2\left(n-1,m\right)} + g_2 m P_{n,m-1}(0)\frac{\sin^2\left[\lambda\left(n,m-1\right)\tau_{\rm int}\right]}{\lambda^2\left(n,m-1\right)}$$

We now have the form of $F\left(\tau\right)$. By plugging it into (3), (4) and rewriting it in terms of the diagonal elements of the density matrix, we get:

$$\dot{P}(n_1,n_2) = 0 = R\{-\sin^2\left[\lambda(n_1,n_2)\tau_{\rm int}\right]P(n_1,n_2) + g_1^2 n_1\frac{\sin^2\left[\lambda(n_1-1,n_2)\tau_{\rm int}\right]}{\lambda^2(n_1-1,n_2)}P(n_1-1,n_2)$$
$$+g_2^2 n_2\frac{\sin^2\left[\lambda(n_1,n_2-1)\tau_{\rm int}\right]}{\lambda^2(n_1,n_2-1)}P(n_1,n_2-1)\}+$$
$$\gamma_1(n_{b1}+1)\left[(n_1+1)P(n_1+1,n_2) - n_1P(n_1,n_2)\right] + \gamma_1 n_{b1}\left[n_1P(n_1-1,n_2) - (n_1+1)P(n_1,n_2)\right] \tag{18}$$

The previous equation contains the probability flow terms between any two successive energy levels cavity field as shown in Fig. 2.

The arrows represent the probability flow between adjacent energy states. Since at steady state, the net probability flow from level (0,0) is zero, we conclude that the sum of the probability flow terms A and B is zero. Under the symmetric operation of the microlaser, defined by,

$$g_1 = g_2, \gamma_1 = \gamma_2, n_{b1} = n_{b2}$$

we can conclude that the probability flow bundles A and B are equal and hence each of them will be identically zero. By induction, one can conclude that the three-term probability flow between any two levels in (18) is zero and we obtain [7]:

$$Rg^2 n_1\frac{\sin^2\left[\lambda(n_1-1,n_2)\tau_{\rm int}\right]}{\lambda^2(n_1-1,n_2)}P(n_1-1,n_2) = \gamma(n_b+1)\left[n_1P(n_1,n_2)\right] - \gamma n_b\left[n_1P(n_1-1,n_2)\right] \tag{19}$$

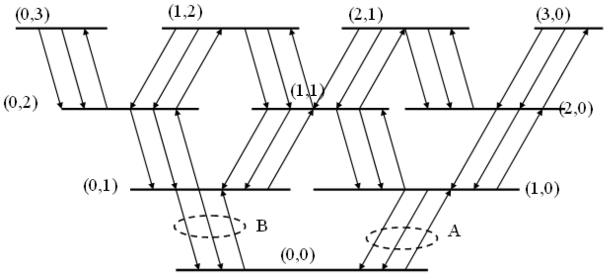

FIG. 2: A schematic diagram of the lowest energy states of the field inside a bi-modal cavity. The arrows represent the probability flow between adjacent energy states.

$$Rg^2 n_2 \frac{\sin^2\left[\lambda(n_1, n_2-1)\tau_{\text{int}}\right]}{\lambda^2(n_1, n_2-1)} P(n_1, n_2-1) = \gamma(n_b+1)\left[n_2 P(n_1, n_2)\right] - \gamma n_b \left[n_2 P(n_1, n_2-1)\right] \tag{20}$$

which can be solved together to get

$$P(n_1, n_2) = P(0,0)\left(\frac{R}{\gamma_1(n_{b1}+1)}\right)^{n_1}\left(\frac{R}{\gamma_2(n_{b2}+1)}\right)^{n_2}\prod_{k=1}^{n_1+n_2}\left(\frac{\gamma n_b}{R} + \frac{1}{k+1}\sin^2\left[g\tau_{\text{int}}\sqrt{k+1}\right]\right) \tag{21}$$

where $P(0,0)$ is obtained from the normalization condition $\sum\limits_{n_1,n_2} P(n_1, n_2) = 1$. The probability to find n photons in one mode regardless of the number of photons in the other mode, $P_\alpha(n)$ is given by

$$\begin{aligned} P_1(n) &= \sum_{n_2} P(n_1, n_2) \\ P_2(n) &= \sum_{n_1} P(n_1, n_2) \end{aligned} \tag{22}$$

We can see easily that $P_1(n) = P_2(n)$, a signature of the symmetric operation of the microlaser. In Fig. 3 , we plot $P_\alpha\,(n)$ for $n_b = 0.1, \frac{R}{\gamma} = 50$ and $g\tau_{\text{int}} = 0.75$, 0.8 and 1. Unlike the photon statistics of the single mode microlaser, we notice in the probability distribution of a single mode of the two-mode microlaser, $P_\alpha\,(n)$ the existence of regions of exactly flat distribution. The explanation for these flat regions is plausible and goes as follows:

The semi-classical rate equation at steady state of the three-level atom microlaser involves the total number of photons in the two modes (n+m) and reads:

$$R\ sin^2\left[g\tau_{\text{int}}\sqrt{n+1+m+1}\right] = \gamma\left[n+m\right] \tag{23}$$

Solutions of (23) specify steady state values for (n+m). Since each value of the solutions for (n+m) can be formed by different combinations of n and m and all these combinations are equally probable, it follows that the probability distribution $P_\alpha\,(n)$ has a flat probability regions corresponding to all the different combinations of n and m. These flat regions are higher for lower n and steps down for larger values of n in a staircase pattern since for every possible solution for (n+m) the possible values of n and m start from zero while the high values of n and m are accessible only for large values of the solutions of (n+m).

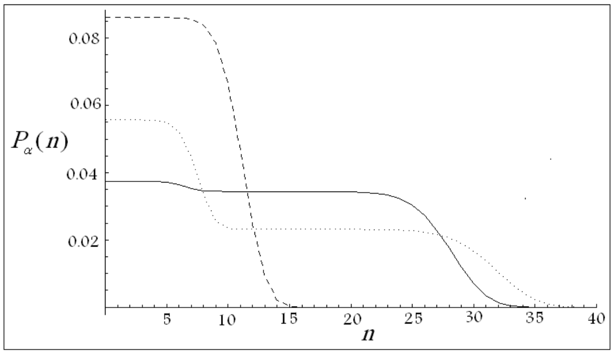

FIG. 3: The photon number probability distribution $P_\alpha\,(n)$for mode 1, calculated for$n_b = 0.1, \frac{R}{\gamma} = 50, g\tau_{\text{int}} =$ 0.75 (dashed), 0.8 (dotted), 1 (solid).

It's notable to say that these flat probability sections are distinctive property of two-mode or higher microlaser. They are responsible for wider probability distribution than the poissonian distribution, i.e., super-poissonian distribution. In the more general case when the coupling between the atoms and the two modes are not identical, $g_1 \neq g_2$, we will have the semi-classical rate equation

$$R\ sin^2\left[\tau_{\text{int}}\sqrt{g_1\,(m+1) + g_2\,(n+1)}\right] = \gamma\left[n+m\right] \tag{24}$$

It's evident that in this case no flat regions will appear in $P_\alpha\,(n)$ since we have a single n and m that satisfy

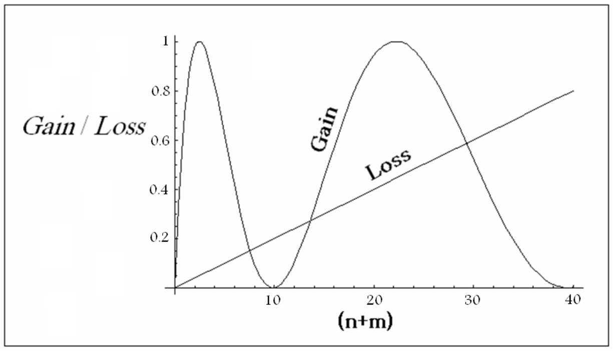

FIG. 4: The gain and loss parts of the semi-classical rate for $g\tau_{\text{int}} = 1, R = 50, \gamma = 1$

the equation. This prediction will be confirmed shortly after applying the Quantum Trajectory Method to the microlaser problem.

A. Second order correlation

The steady state of the microlaser, as implictely mentioned above, doesn't mean that the field inside the cavity of a certain microlaser setup has a fixed radiation intensity (i.e., a definite number of photons) since each atom will induce a change in the field and the field decay between two atoms induces further changes in the field or the number of photons. We are interested in this part to examine the correlation between these fluctuations in the cavity field, or more precisely, fluctuations in the number of photons inside the cavity represented by the second order correlation function $g^{(2)}(\tau)$. Measurement of the correlation function of the cavity field may provide a direct evidence of the quantized nature of light by detecting distinct correlation effects of the quantum field such as photon anti-bunching. The second order correlation function of the quantized field inside the cavity, $g^{(2)}(\tau)$, is proportional to the probability of finding a pair of photons inside the cavity separated by a time τ [11], regardless of what happens to the photon number during this time interval and is defined by:

$$g^2(\tau) = \frac{\langle a^\dagger(0)a^\dagger(\tau)a(\tau)a(0)\rangle}{\langle n\rangle^2} \tag{25}$$

The correlation function of a micromaser cavity field can be calculated analytically as shown by Quang [14] by starting with a density matrix $\tilde{\rho}(0)$, conditioned on the act of detecting and annihilating a photon from the cavity field.

$$\tilde{\rho}(0) = \frac{a\rho_{ss}a^\dagger}{Tr\left[a\rho_{ss}a^\dagger\right]}$$

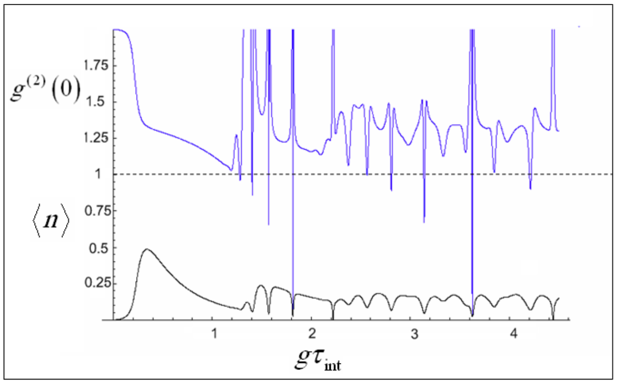

FIG. 5: The initial value of the second order correlation function $g^{(2)}(0)$ and the normalized mean photon number plotted versus the pump parameter θ for a two-mode microlaser

where ρ_{ss} is the steady state solution of the master equation. We evolve this conditional density matrix by the micromaser master equation and the correlation function at time τ will be proportional to the mean number of photons inside the cavity at time τ as calculated by the evolved conditional density matrix $\tilde{\rho}(\tau)$.

$$g^{(2)}(\tau) = \frac{Tr\left[a^\dagger a\tilde{\rho}(\tau)\right]}{\langle n\rangle}$$

To calculate the evolution of the conditional density matrix $\tilde{\rho}(\tau)$, we solve the master equation by 4th order Runge Kutta Method. The quantum regression theorem has been used to derive this method. The other method to calculate $g^{(2)}(\tau)$ mimics what is done experimentally and is based on calculating the correlation between the times at which photons leak from the cavity. We will use the second method in the next section to calculate $g^{(2)}(\tau)$ numerically by the Quantum Trajectory Method.

When we plot the initial value of the correlation function of any of the two modes versus the pumping parameter $g\tau_{\text{int}}$, we notice as shown in Fig. 5 that $g^{(2)}(0)$ is always higher than one except at the photon trapping states [15] occurring at the severe dips in $g^{(2)}(0)$ and in the normalized mean number of photons $\langle n\rangle$. This means that photon number probability distribution $P_\alpha(n)$ is super-poissonian for most of the range of $g\tau_{\text{int}}$, a consequence of the flatness of $P_\alpha(n)$ explained earlier. This situation is not the same in the single mode microlaser due to the absence of this flatness. We depict in Fig. 6 the same graph for the single mode microlaser where the normalized mean number of photons and $g^{(2)}(0)$ are plotted versus the pumping parameter θ defined by:

$$\theta = g\tau_{\text{int}}\sqrt{N_{ex}}$$

and

$$N_{ex} = R/\gamma$$

It's evident that the photon number distribution exihibits both sub-poissonian and super-poissonian statistics in the single mode microlaser.

In the rest of this section we are going to concentrate on the correlation function at the trapping states defined

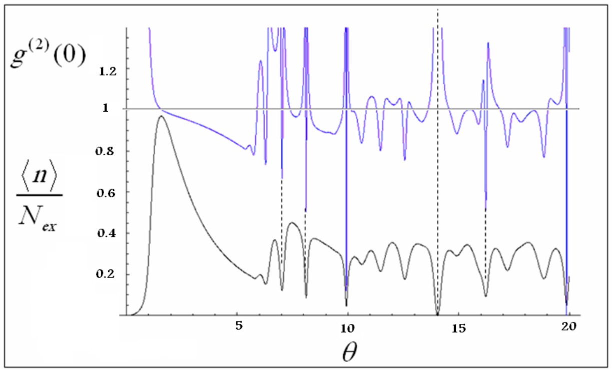

FIG. 6: The initial value of the second order correlation function $g^{(2)}(0)$ and the normalized mean photon number plotted versus the pump parameter θ for a single-mode microlaser

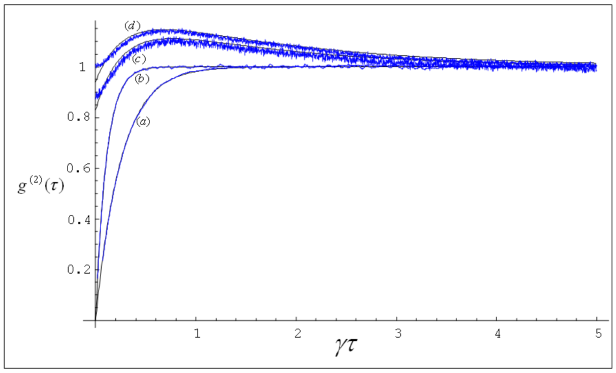

FIG. 7: The second order correlation function $g^{(2)}(\tau)$ corresponding to $g\tau_{\text{int}} = \frac{\pi}{\sqrt{3}}$(a), $\frac{2\pi}{\sqrt{3}}$(b), $\frac{\pi}{\sqrt{5}}$(c)and $\frac{\pi}{\sqrt{6}}$(d) calculated by QTM and compared with the analytical method

by the condition $g\tau_{\text{int}}\sqrt{n+1+m+1} = k\pi$ for a certain (n+m). At these states, the probability to find numbers of photons larger than (n+m) will be identically zero since the probability for each atom to emit its photon while interacting with the cavity field is proportional to $sin^2\left[g\tau_{\text{int}}\sqrt{n+1+m+1}\right]$. A trapping state is characterized by a sharp dip- called resonance- in the mean number of photons inside the microlaser cavity plotted versus the pumping parameter $g\tau_{\text{int}}$. In Fig. 7 we show $g^{(2)}(\tau)$ calculated for the one, three and four photon trapping states and compared with the numerical calculation by the Quantum Trajectory Method. Severe anti-bunching is noticed for the one-photon trapping state.

We can understand the anti-bunching behavior of the one photon trapping state in terms of the necessary time needed between detecting a photon out from the cavity and re-pumping the cavity by an excited atom that deposits another photon inside. This dead time between detecting a photon and re-pumping the cavity is responsible for the photons anti-bunching. This situation is very similar to the anti-bunching of the fluorescence radiation emitted by a single atom where a dead time is unavoidable between the emission of a photon and re-exciting

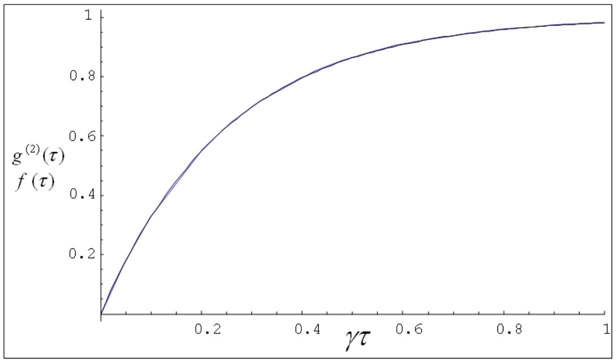

FIG. 8: The second order correlation function $g^{(2)}(\tau)$ fitted with the analytical function $f(\tau)$

the atom. We know from the theory of resonance fluorescence of a single atom that the expression of the second order correlation $g^{(2)}(\tau)$ of the radiation scattered by a two-level atom driven by arbitrary field is given by [11, 12]

$$g^{(2)}(\tau) = 1 - \left(\cos\mu\tau + \frac{3\gamma}{4\mu}\sin\mu\tau\right)e^{-\frac{3\Gamma}{4}\tau}$$

where Γ is the spectral linewidth of the atom, or alternatively its spontaneous decay rate and μ is defined in terms of Γ and the Rabi frequency Ω_R by $\mu = \sqrt{\Omega_R^2 - \frac{\Gamma^2}{16}}$

The analogy between the two-level atom and the one-photon trapping state is clear. The cavity plays the role of a two-level system where the two levels are either a photon is stored in the cavity or not. The difference between the two systems is in the method of pumping and decaying from the higher level to the lower level. While the atom undergoes continuous Rabi oscillation by the pumping laser field, the cavity is pumped by a stream of atoms arriving randomly and separated by relatively large intervals. Probably this is the reason of not having the oscillatory behavior in the correlation function of the cavity field. We tried to fit $g^{(2)}(\tau)$ for this particular case with an analytical function and found that the function $1-e^{-\eta\tau}$, where $\eta = R\ sin^2\left[g\tau_{\text{int}}\sqrt{2}\right] + \gamma$ fits excellently with $g^{(2)}(\tau)$ as shown in Fig. 8. We found that the correlation function for the total number of photons (in the two modes) exhibits the same behavior and can be fitted with the same function. This behavior is not pertinent to the two-mode microlaser, but appears also in the single-mode microlaser operating in its one photon trapping state characterized by $sin^2\left[g\tau_{\text{int}}\sqrt{1+1}\right] = 0$. We found that its correlation function fitted excellently with the analytical function

$$f(\tau) = 1 - e^{-\eta\tau}, \tag{26}$$

where $\eta = R\ sin^2\left[g\tau_{\text{int}}\sqrt{1}\right] + \gamma$. We give a proof of this relation in the appendix

III. APPLYING THE QUANTUM TRAJECTORY METHOD TO SOLVE THE THREE-LEVEL ATOM MICROLASER

A numerical method, basically a Monte Carlo simulation applied to quantum systems, to solve dissipative master equations was developed by three groups nearly at the same time in the early nineties [8, 9, 10, 11]. In this method, called Quantum Trajectory Method (QTM), the observables of the system are obtained by averaging over many possible histories of the evolution of the system density matrix as a function of time. Each of these histories is called a trajectory, and its evolution is of a stochastic nature. Due to the statistical nature of quantum mechanics, taking the average over a large number of trajectories is equivalent to solving the master equation for this system. This is the essence of the quantum trajectory method. A certain trajectory can describe the stochastic evolution of the wavefunction or the density matrix of the open quantum system subjected to random quantum jumps representing its interaction with the reservoir. This method has a numerical advantage by reducing the computational power required to solve the master equation by the order of the dimension of the system, especially when the system has many degrees of freedom [9]. Another advantage of the quantum trajectory method is the high level of control it allows on the parameters of the system. In our case we will use this ability to let each atom in any trajectory have a different velocity according to the velocity probability distribution, simulating what happens in reality. Including the variation of the atoms' speeds in the analytical solution of the master equation is a difficult task. Instead of evolving the density matrix in each trajectory, we will evolve wavefunctions representing the state of the cavity field. The simplest wavefunction one can use to represent the quantized electromagnetic field is the number state [10]. For this reason and generalizing the quantum trajectory algorithm applied to the single mode micromaser developed by Pickles and Cresser in [10], we evolve two number states $|m\rangle$, |n$\rangle$ representing the deterministic number of photons in the two modes. In the most general case, where the two-mode micromaser cavity is maintained at a very low temperature, we can infer seven different events that may occur to the number state $|m,n\rangle$ with the following probabilities:

1-An atom emits a photon in the first mode: $|m,n\rangle \rightarrow |m+1,n\rangle$ with probability: $\frac{1}{A}R\,(m+1)\,g_1^2\,\sin^2\left[\lambda(m,n)\tau_{\text{int}}\right]/\lambda^2(m,n)$

2- An atom emits a photon in the second mode: $|m,n\rangle \rightarrow |m,n+1\rangle$with probability: $\frac{1}{A}R\,(n+1)\,g_2^2\,\sin^2\left[\lambda(m,n)\tau_{\text{int}}\right]/\lambda^2(m,n)$

3- A photon from the first mode leaks out from the cavity $|m,n\rangle \rightarrow |m-1,n\rangle$, with probability $\frac{1}{A}\gamma_1(n_{b_1}+1)m$

4- A photon from the second mode leaks out from the cavity $|m,n\rangle \rightarrow |m,n-1\rangle$, with probability $\frac{1}{A}\gamma_2(n_{b2}+1)n$

5- A photon from the cavity walls is transferred to the cavity field of the first mode, $|m,n\rangle \rightarrow |m+1,n\rangle$ with probability $\frac{1}{A}\gamma_1 n_{b_1}\,(m+1)$

6- A photon from the cavity walls is transferred to the cavity field of the second mode, $|m,n\rangle \rightarrow |m,n+1\rangle$ with probability $\frac{1}{A}\gamma_2 n_{b_2}\,(n+1)$

7- An atom passes through the cavity without emitting any photons, $|m,n\rangle \rightarrow |m,n\rangle$, with probability $\frac{1}{A}R\cos^2\left[\lambda(m,n)\tau_{\text{int}}\right]$ where

$$A = R + \gamma_1\left[(n_{b_1}+1)m + n_{b_1}(m+1)\right] + \gamma_2\left[(n_{b_2}+1)n + n_{b_2}(n+1)\right]$$

The values of these probabilities can be derived by writing the master equation in the Lindblad form

$$\dot{\rho} = -\frac{i}{\hbar}\left[\hat{H},\rho\right] + \sum_m\left[\hat{C}_m\rho\hat{C}_m^\dagger - \frac{1}{2}\left(\hat{C}_m\hat{C}_m^\dagger\rho + \rho\hat{C}_m^\dagger\hat{C}_m\right)\right] \tag{27}$$

where $\hat{C}_m$ represents the jump operator representing event (m). The probability of event (m) is calculated by:

$$p(m) = \frac{\langle\psi(t_1)|\,\hat{C}_m^\dagger\hat{C}_m\,|\psi(t_1)\rangle}{\sum\limits_m\langle\psi(t_1)|\,\hat{C}_m^\dagger\hat{C}_m\,|\psi(t_1)\rangle} \tag{28}$$

and the waiting time between two successive jumps probability distribution function is given by:

$$p(\tau) = e^{-\int\limits_t^{t+\tau}\sum\limits_m\langle\psi(t)|\hat{C}_m^\dagger\hat{C}_m|\psi(t)\rangle dt}$$

and for our system $p(\tau)$ becomes ,

$$p(\tau) = e^{-A\tau}$$

The choice of number states as the propagated wavefunctions has the advantage that the effective Hamiltonian controlling the evolution of the wavefunction between jumps keeps the number states unchanged [10]. For more on the Quantum Trajectory Method, see [8, 9, 11].

After generating many trajectories, we determine the diagonal elements of the density matrix by making a histogram over the final states $|m,n\rangle$ of each trajectories.

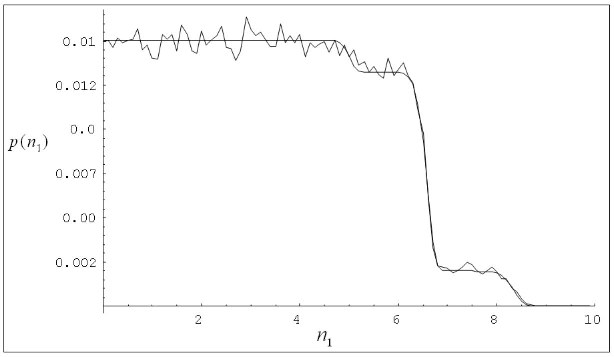

FIG. 9: The photon number probability distribution $P_\alpha\left(n\right)$for mode 1 calculated numerically and compared to the analytical solution for $R/\gamma = 200,\ g\tau = 0.3$

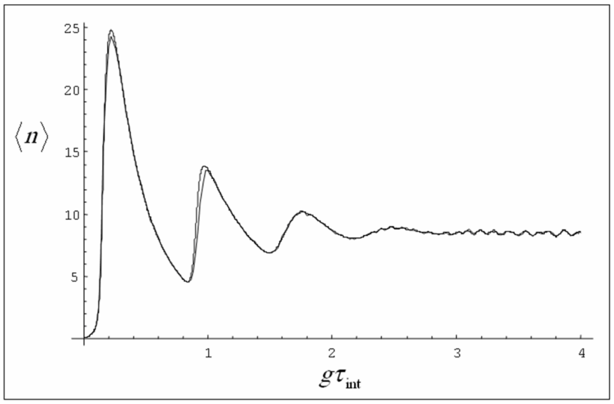

FIG. 10: The mean number of photons in mode 1 calculated numerically and compared to the analytical solution

We show the photon number probability distribution calculated by the Quantum Trajectory Method for a microlaser operating at $R/\gamma = 200,\ g\tau = 0.3$ in Fig. 9 where QTM shows an acceptable accuracy.

The accuracy becomes better for lower values of R/γ . In Fig. 10 we show the mean number of photons in one mode versus $g\tau_{\text{int}}$ obtained numerically and analytically. We used QTM to confirm that a microlaser operating in the non-symmetric mode, where the detailed balance condition doesn't apply, does reach steady state by checking that the avergae steady state density matrix calculated by QTM is the same when taking different lengthes of the trajectories.

In fig. 11 we see clearly that the flat regions disappear in the non-symmetric operation of the microlaser as predicted earlier. It turns out that this flatness in $P_\alpha\left(n\right)$ is very sensitive to the difference between the coupling constants of the two modes as in fig. 12.

To calculate the second order correlation function using the Quantum Trajectory Method, we use a numerical method similar to the one used experimentally [16]. In the experiment conducted by the group of M. Feld in MIT, the coherence function of the microlaser is obtained by calculating the correlation between the times

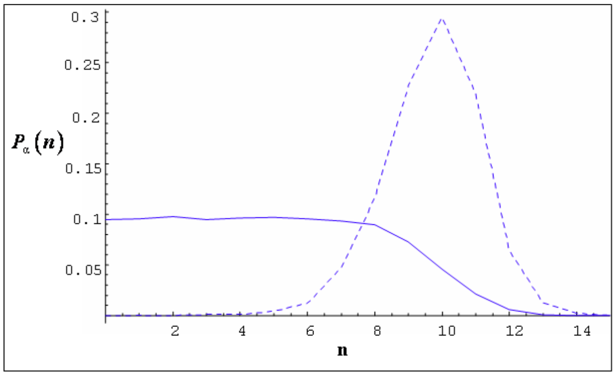

FIG. 11: The photon number probability distribution calculated numerically for $g_1 = g_2 = 0.8$ (solid) and $g_1 = 0.8, g_2 = 0.5$ (dashed)

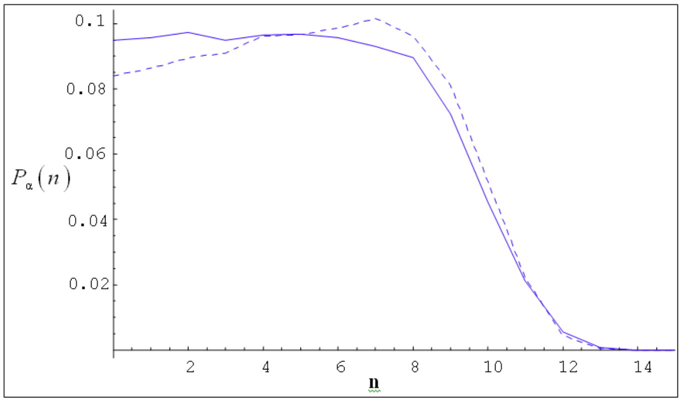

FIG. 12: The photon number probability distribution calculated numerically for $g_1 = g_2 = 0.8$ (solid) and $g_1 = 0.8, g_2 = 0.79$ (dashed)

when photons are emitted out from the cavity and detected by the photo-detector. Numerically, we have full details about each trajectory including the times at which photons leak from the cavity. So to calculate $g^{(2)}(\tau)$, we compute the correlation between these times in each trajectory and average over all the trajectories. We have already shown in Fig. 7 the numerical calculation of $g^{(2)}(\tau)$ compared with the analytical calculation for the trapping states where $g^{(2)}(\tau)$ exhibits anti-bunching behavior. We show in Fig. 13 the correlation function for two values of $g\tau_{\text{int}}$ where the cavity field exhibits bunching behavior. In Fig. 14 we illustrate an interesting feature of $g^{(2)}(\tau)$ where the cavity field exhibits a transient anti-bunching behavior before it decays monotonically to one.

IV. EFFECT OF ATOMIC VELOCITY DISTRIBUTION ON THE STATISTICAL PROPERTIES OF THE MICROLASER

As we mentioned briefly in the introduction, atomic velocity selectors are not perfect and eventually the atoms

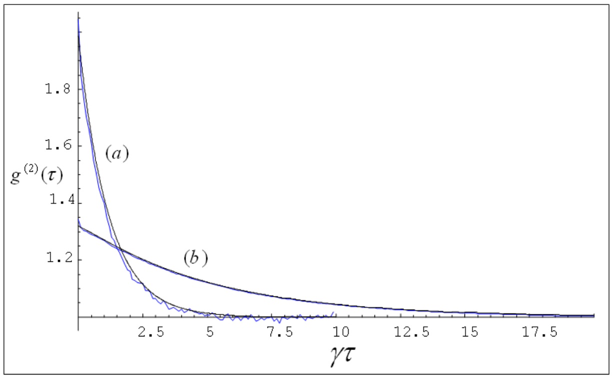

FIG. 13: The second order correlation function $g^{(2)}(\tau)$ calculated for $n_b = 0, \frac{R}{\gamma} = 10$, $g\tau_{\rm int} = 0.12$ (a) and 0.5 (b) numerically and analytically.

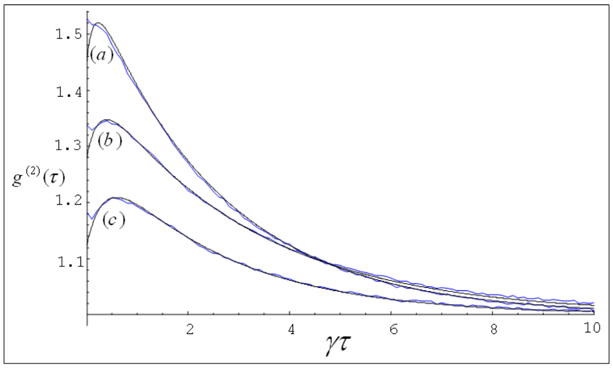

FIG. 14: The second order correlation function $g^{(2)}(\tau)$ calculated for $n_b = 0, \frac{R}{\gamma} = 10$, $g\tau_{\rm int} = 3$ (a), 2 (b) and 1 (c) numerically and analytically.

passing through the microlaser cavity will have some velocity distribution. In this section, we are going to illustrate the effect of this velocity spread of the atoms on the statistical properties of a single field mode of the microlaser cavity. It might be expected that the velocity spread of the atoms will destroy the flat probability regions highlighted in the previous sections, but a quick look at Fig. 3 tells us that this is not correct. In fact, including a variety of interaction times is going to average the flat regions in the probability distribution corresponding to each value of $\tau_{\rm int}$ and we end up with a persistent flat probability distribution whose width and height is a function of the relative atomic velocity spread as shown in Fig. 15. In this figure, we show that a relative velocity spread of 20% maintains the flat regions in $P_\alpha(n)$, corresponding to $g\tau_{\rm int}$=0.8 and $r/\gamma = 50$.

A vacuum trapping state is special trapping state where the cavity field is trapped at the vacuum state and occurs when the condition $g\tau_{\rm int}\sqrt{1+1} = n\pi$ applies. This state, like other trapping states is characterized by a sharp dip in the plot of the mean number of photons. It is evident that the randomness in the interaction time $\tau_{\rm int}$will destroy this condition and remove the resonances

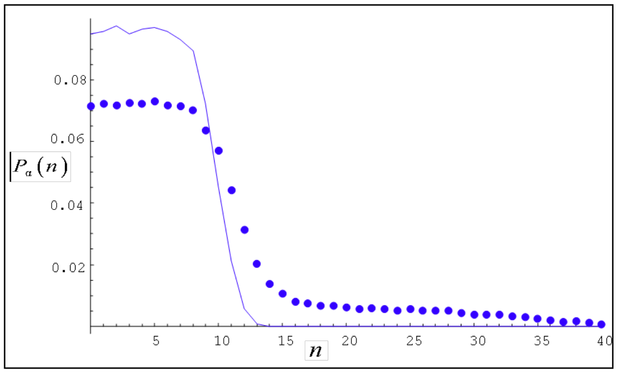

FIG. 15: The photon number probability distribution calculated numerically for the case of pumping the microlaser with a mono-velcoity atomic beam (solid) and an atomic beam having relative velocity spread of 20% (dotted)

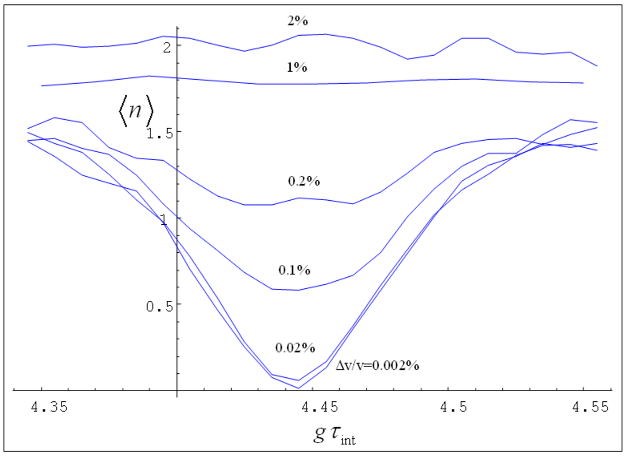

FIG. 16: The mean number of photons at a trapping state for different relative velocity spreads.

from the microlaser behavior. This is shown in Fig. 16 where the mean number of photons in a vacuum trapping state is plotted for relative velocity distribution widths of .002%, .02%, .1%, 0.2%, 1% and 2%. It is notable that the trapping state is very sensitive to velocity distribution width.

We noticed the existence of sharp transitions in the mean number of photons plotted versus $g\tau_{\rm int}$ in Fig. 10. These transitions occur between stationary solutions of the semi-slassical rate equation and we expect them to be induced by the randomness involved in the quantum system. We noticed, however, that including the spread in the atoms' velocities and hence increasing the randomness in the interaction times destroys these transitions starting from the transitions at large values of $g\tau_{\rm int}$ which are very sensitive to the velocity broadening. We show this behavior in Fig. 17 where the mean number of photons is plotted versus $g\tau_{\rm int}$ for a Guassian distribution of width 60%. This plots confirm that the system becomes more classical as more velocity fluctuations are introduced [17]. We can understand the immunity of

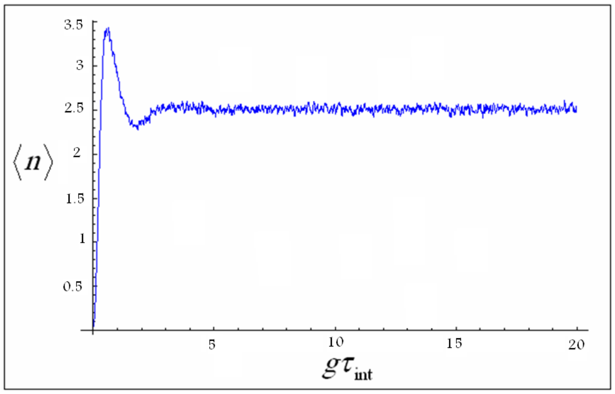

FIG. 17: The mean number of photons of the two-mode microlaser when relative velocity spreads of 60% is included

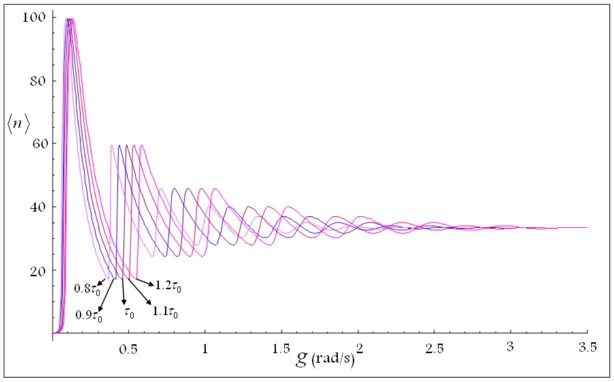

FIG. 18: The mean number of photons plotted versus the coupling constant g for different values of the interaction times to illustrate how a distribution of the interaction times (or equivalently atomic velocities) affect the microlaser phase transitions. τ_0 is an arbitrary value of the interaction time equal to 1 s. The figure is for illustration and the values of g and τ_0 are not realistic.

the first transition to the velocity distribution and the fragility of the peaks at higher values of $g\tau_{\rm int}$ by plotting the mean number of photons versus g for different values of the interaction times $\tau_{\rm int}$. We see from the plots in Fig. 18, which correspond to a relative velocity spread of 40%, why the first phase transition is not much affected while the higher transitions are easily destroyed.

A. Effect of velocity spread on the correlation function

We have seen in the theory of the three-level two-mode microlaser that the photon statistics of the cavity field exhibits bunching behavior for most of the range of the pumping parameter except at some of the trapping states, where the field is anti-bunched. We are going to show now the effect of the velocity spread on the second order coherence function in the two cases. We distinguish two regions from Fig. 5: the first is the smooth region where $g^{(2)}(0) < 2$ and the second one is the sharp peaks of $g^{(2)}(0)$ at the vacuum trapping states where $g\tau_{\rm int}$ is multiple of $\pi/\sqrt{3}$. For the first case, we observed that the correlation is very immune to the atomic velocity spread and even a very broad velocity distribution doesn't reduce the field correlation substantially as shown in Fig. 19 where the correlation due to mono-velocity atomic beam for a microlaser operating at $g\tau_{\rm int} = 0.6$ and R = 10 is compared with microlaser pumped by an atomic beam having a spread of $\frac{\Delta v}{v_o} = 0\%,\ 20\%,\ 50\%$ and 100%. While increasing the velocity spread changes the average velocity for the atoms and hence drifts the operating point of the microlaser slightly, what we want to emphasize from Fig. 19 is that correlation is not affected much by the velocity spread.

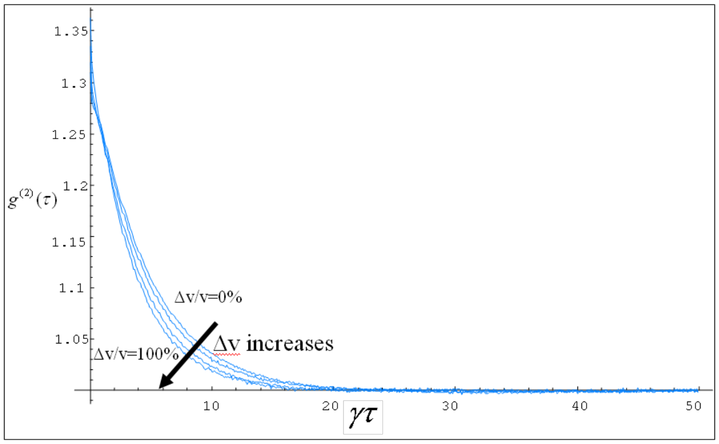

FIG. 19: Second order correlation function for different atomic velocity spreads far from a trapping state $\frac{\Delta v}{v_o} = 0\%, 20\%, 50\%$ and 100%.

Finite correlation for practical atomic beams of relative velocity spreads upto 20% has indeed been measured for the single-mode microlaser by Aljalal [16]. As for the regions near the vacuum trapping states, $g^{(2)}(0)$ is peaked because the number of photons inside the cavity is very small. The correlation function at these regions is strongly bunched which means that whenever a few number of photons happen to exist inside the cavity, they will tend to leave the cavity together as a bunch of photons. At the extreme case of the vacuum trapping state, the correlation function diverges since the cavity has no photons. We noticed that when operating the cavity near a vacuum trapping state where $g^{(2)}(0)$ is very large, the correlation is very sensitive to the velocity spread of the atoms and collapses very fast until some residual correlation persists at a relative velocity spread of 2%. In Fig. 20 we show the second order correlation function of the cavity field $g^{(2)}(\tau)$ for a microlaser operated close to this state ($g\tau_{\rm int} = 1.994\pi/\sqrt{3}$). In this figure, $g^{(2)}(\tau)$ of a mono-velocity beam is shown in addition to velocity spreads $\frac{\Delta v}{v_o}$ of 0.02%, 0.03%, 0.04%, 0.06%, 0.08%, 0.1%, 0.2% and 2%. We note that the correlation length has approximately the same value for first six values of

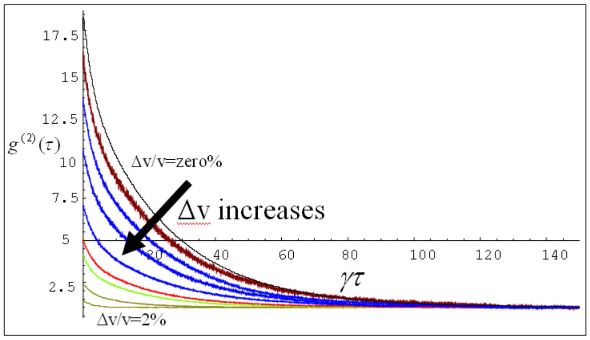

FIG. 20: The second order correlation function for different velocity spreads near a vacuum trapping state $\frac{\Delta v}{v_o}$= 0.02%, 0.03%, 0.04%, 0.06%, 0.08%, 0.1%, 0.2%, 2%.

$\frac{\Delta v}{v_o}$. The reason for the fragility of the correlation near a vacuum trapping state to the atomic velocity spread is that the smallest distribution in the interaction times destroys the vacuum trapping state as we saw in Fig. 16 and will introduce a small number of photons inside the cavity. These photons will cause the residual correlation mentioned above. Increasing the relative velocity spread beyond 2% doesn't affect this residual correlation considerably as in the first case (non-trapping states) where the correlation is very immune to the atomic velocity spread.

On the other hand, when we investigated the effect of the atomic velocity spread on the correlation function for an operating point exhibiting anti-bunching, i.e., the one-photon trapping state, we found an interesting phenomenon. Adding more fluctuations in the atoms' velocity, produces a peak in the correlation function near $\tau = 0$ and the field gradually becomes more correlated up to a relative velocity spread of $\frac{\Delta v}{v_o} = 0.2\%$ as shown in Fig. 21. In other words, the anti-bunching is converted into bunching. The explanation of this weird behavior of noise-induced correlation goes as follows: when the velocity spread is slightly increased starting from the mono-velocity case, there will be a very small probability to find numbers of photons inside the cavity higher than one photon, i.e., a bunch of photons. Although the probability is very small compared to the probability to find one photon or zero photon, its effect is overwhelming and eventually the correlation function is dominated by these rare bunches of photons that can exist inside the cavity.

In a quantitative way, we can explain it from the initial value $g^{(2)}(0)$ which is given by [14]:

$$g^{(2)}(0) = \frac{\langle n^2\rangle - \langle n\rangle}{\langle n\rangle^2}$$

. For the one photon trapping state, we have $P(0), P(1) \neq 0$ and $P(n) = 0$ for $n > 1$ and hence $\langle n^2\rangle = \langle n\rangle = P(1)$ This makes $g^{(2)}(0) = 0$. For the slightest velocity distribution, the trapping state will be destroyed and $P(n)$ will no longer be 0 for n>1. This makes $g^{(2)}(0) > 0$ as we see from Fig. 21. We can illustrate this by a numerical example, for the case of a relative velocity spread of .01%. We find in this case from the QTM simulation that $P(n) > 0$ for $n \leq 7$ and $\langle n\rangle = 0.3918$ and $\langle n^2\rangle = 0.4264$. These values yield an initial value of the correlation function $g^{(2)}(0)$ to be 0.2254. It turns out that the wider the velocity distribution, the higher the value of $g^{(2)}(0)$ is till Δv/v reaches 0.2%. By increasing the relative velocity spread above 0.2%, the correlation is lost gradually due to the huge randomness in the interaction times between the atoms and the cavity, until a residual correlation persists starting from a relative velocity spread of 20%. This is clear in Fig. 22 where we notice that correlation and hence the bunching of the cavity photons decreases gradually for relative velocity spreads of 0.2%, 0.6%, 1%, 2% and 20%. Next, we show the effect of velocity distribution on the correlation function of the total number of photons in the cavity (i.e., in the two modes combined). With a velocity spread of 0.4%, and $g\tau_{\text{int}} = \frac{\pi}{\sqrt{3}}$ and $\frac{2\pi}{\sqrt{3}}$, we get the plots shown in Fig. 23 where as in Fig. 21, we notice that the anti-bunching behavior in $g^{(2)}(\tau)$ has been converted into bunching for the same reason mentioned above.

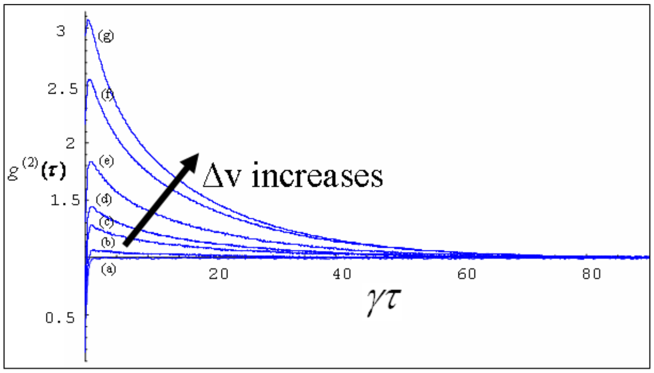

FIG. 21: The second order correlation function for a one-photon trapping state and relative velocity spreads Δv/v = 0.01% (a), 0.03% (b), 0.05% (c),0.07% (d), 0.1% (e), 0.15% (f) and 0.2% (g)

V. CONCLUSION

We have applied the Quantum Trajectory Method to the two mode microlaser operating on Λ-type three level atoms. We verified that the two-mode microlaser does reach steady state when the coupling between the atom and the two modes is not symmetric, the case where the detailed balance condition doesn't apply. As for the symmetric operation of the microlaser, we explained the flat probability regions in the photon number probability distribution of any of the two modes and emphasized the fact that the existence of two modes equally coupled to the atoms gives rise to these flat regions. The super-poissonian distribution of the photon statistics of any of the two modes is a direct consequence of these flat re-

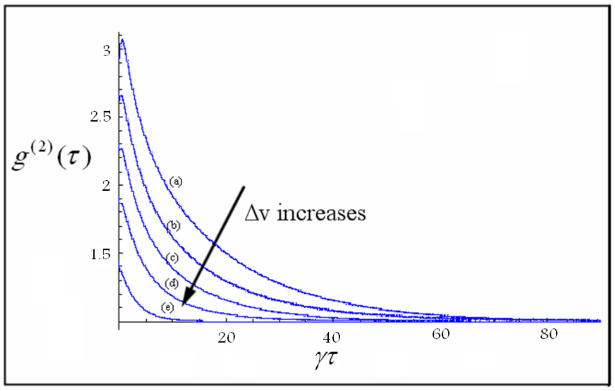

FIG. 22: The second order correlation function for a one-photon trapping state and relative velocity spreads $\Delta \mathrm{v}/\mathrm{v} = 0.2\%(\mathrm{a}), 0.6\%(\mathrm{b}), 1\%(\mathrm{c}), 2\%(\mathrm{d})\mathrm{and} 20\%(\mathrm{e})$The microlaser is operated at $g\tau_{\mathrm{int}} = 1.81379, \mathrm{R} = 10, \mathrm{n_b}= 0$

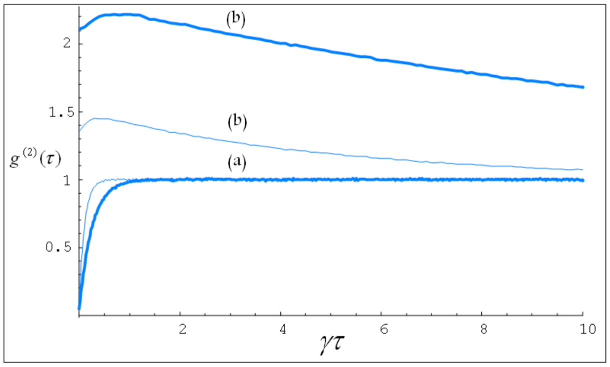

FIG. 23: The second order correlation function for the total number of photons for the one-photon trapping states $g\tau_{\mathrm{int}} = \pi/\sqrt{3}$ (thick) and $2\pi/\sqrt{3}$ (thin) and relative velocity spreads $\Delta \mathrm{v}/\mathrm{v} = 0\%$ (a) and 0.04% (b)

gions and causes the photon correlation to be bunched for most of the range of the operating parameters of the microlaser, a distinct property that distinguishes the two-mode microlaser from the single mode microlaser. We introduced the analogy between the correlation of the field of the one-photon trapping state and the resonance fluorescence radiation scattered from a two-level atom. We fitted the correlation function of this state to a very simple formula and give an analytical derivation of this formula in the appendix. Experimental measurement of this anti-bunching is a direct verification of the quantized nature of the field. We investigated the effect of the atomic velocity spread on the photon statistics by the Quantum Trajectory Method. We found that the trapping states are very sensitive to the velocity spread of the atoms. The sharp transitions in the microlaser output are also destroyed by the velocity distribution of the atoms starting from the transitions at higher values of the pumping parameter. The second order correlation is in general immune to the velocity spread of the atoms. For the special case when the microlaser is operating near a vacuum trapping state, the intensity correlation of the cavity field is easily destroyed by a relative velocity spread as low as 0.2 %. Increasing the velocity spread further doesn't affect the low residual correlation that survives the velocity spread of the atoms. When the cavity field of the mono-velocity atomic beam microlaser exhibits anti-correlation, adding randomness in the atomic velocities counter-intuitively converts the anti-correlation into correlation. This noise-induced correlation stops at velocity spreads of about 0.2 %. Increasing the velocity spread further destroys the correlation very slowly until a residual correlation persists for relative velocity spreads of 20% and higher.

We propose as a further investigation developing a quantum trajectory method from the Fokker-Planck equation of the microlaser [17] and evolving coherent states of radiation instead of number states, as the coherent states are the closest states to the classical radiation field.

The quantized motion of the atom inside the cavity could possibly be included in the numerical simulation by quantizing the longitudinal dimension of the cavity and involving the position of the atom in the wavefunction we propagate by QTM during the atom field interaction. The quantized motion of the atom inside the cavity was shown to lead to some distinct features of the two-mode micromaser [18].

Lastly, we would like to propose a novel numerical method to solve the master equation of the microlaser by using a Genetic Algorithm. The basic idea behind using Genetic Algorithms to solve complex problems is to generate an initial random ensemble of solutions and then apply some criterion or fitness condition to select some of them that are closer to the proper solution of the problem. These good candidates are merged together, swapped, paired, or mutated to form another generation of solutions upon which we apply the same fitness criterion to select the good candidates and repeat this cycle till we obtain the best fitting solution to the problem. When applying this algorithm to the microlaser, the elements of the ensemble of solutions will be the density matrices representing the steady state field statistics. The criterion would be minimizing the change incurred to the matrix when an atom passes through the cavity and the field is let to decay. The ideal solution should have zero change from the definition of the micromaser steady state. We select the good candidates of any generation of solutions by picking the matrices that yield the minimum of this change. Merging a set of matrices together to bring up another generation of solutions should be an easy numerical task.

APPENDIX

We are going to prove that for the one photon trapping state, $g^{(2)}(\tau)$ is exactly equal to $f(\tau)$ given in (26) for the case of the two level single mode microlaser since it's much easier than the two-mode case. Starting from the definition of $g^{(2)}(\tau)$ for a quantized field:

$$g^{(2)}(\tau) = \frac{\langle a^{\dagger}(0)a^{\dagger}(\tau)a(\tau)a(0)\rangle}{\langle n\rangle^{2}} \tag{A.1}$$

where $\tau = 0$ represents the steady state. For the one photon trapping state only the states $|0\rangle, |1\rangle$ are accessible to the cavity field. We can then write

$$\begin{aligned} g^{(2)}(\tau) &= \frac{\sum\limits_{n=0,1} \langle n| a^{\dagger}(0)a^{\dagger}(\tau)a(\tau)a(0)|n\rangle}{\langle n\rangle^{2}} \\ &= \frac{\sum\limits_{n=0,1} n.\langle n-1| a^{\dagger}(\tau)a(\tau)|n-1\rangle}{\langle n\rangle^{2}} \\ &= \frac{\langle 0| a^{\dagger}(\tau)a(\tau)|0\rangle}{\langle n\rangle^{2}} \\ &= \frac{\langle 0| \hat{n}(\tau)|0\rangle}{\langle n\rangle^{2}} \end{aligned} \tag{A.2}$$

where $\hat{n}(\tau)$ is the number operator $a^{\dagger}(\tau)a(\tau)$. Under the one-photon trapping state condition, we have only two possibilities: to find 0 or 1 photon inside the cavity and hence

$$n(t) = \sum_{n} n.p_n(t) = p_1(t) \tag{A.3}$$

since $p_n(t) = 0$ for $n \neq 0, 1$. It can be shown from the single mode microlaser master equation (see for example [14]) that evolution of $p_1(t)$ is governed by:

$$\dot{p}_1(t) = p_0(t)R\sin^2\left[g\tau_{\text{int}}\sqrt{1}\right] - \gamma p_1(t) \tag{A.4}$$

From (A.4, A.3), we deduce that the evolution of the mean number of photons inside the cavity is governed by

$$\dot{n}(t) = p_0(t)R\sin^2\left[g\tau_{\text{int}}\sqrt{1}\right] - \gamma n(t) \tag{A.5}$$

This equation is intuitive for the one-photon trapping state and could have been written directly without referring to master equation. The second term on the left hand side represents the rate of photon loss from the cavity while the first term represents the number of photons injected inside the cavity per unit time. At steady state, $\dot{p}_1(0) = 0$ and hence

$$0 = \{1 - p_1(0)\}R\sin^2\left[g\tau_{\text{int}}\sqrt{2}\right] - \gamma p_1(0)$$

which leads to

$$\langle n\rangle = \langle n^2\rangle = p_1(0) = \frac{R\sin^2\left[g\tau_{\text{int}}\sqrt{2}\right]}{\gamma + R\sin^2\left[g\tau_{\text{int}}\sqrt{2}\right]} \tag{A.6}$$

Since $p_1(t) + p_0(t) = 1$, we can write (A.5) as:

$$\dot{n}(t) = (1 - n(t))\,R\sin^2\left[g\tau_{\text{int}}\sqrt{2}\right] - \gamma n(t)$$

.

$$= R\sin^2\left[g\tau_{\text{int}}\sqrt{2}\right] - \left(R\sin^2\left[g\tau_{\text{int}}\sqrt{2}\right] + \gamma\right)n(t)$$

.

$$= A - Bn(t) \tag{A.7}$$

where

$$A = R\sin^2\left[g\tau_{\text{int}}\sqrt{2}\right], B = \left(R\sin^2\left[g\tau_{\text{int}}\sqrt{2}\right] + \gamma\right) \tag{A.8}$$

By integrating (A.7) from $0 \to \tau$ we get

$$\int\limits_{n(0)}^{n(\tau)} \frac{dn}{A - B.n} = \int\limits_{0}^{\tau} dt \tag{A.9}$$

By solving for $n(\tau)$, we obtain:

$$n(\tau) = \frac{A}{B} - \left[\frac{A}{B} - n(0)\right]e^{-B\tau} \tag{A.10}$$

Since we know that

$$n(0) = \sum_{n} \langle n| \hat{n}(0)|n\rangle \tag{A.11}$$

$$n(\tau) = \sum_{n} \langle n| \hat{n}(\tau)|n\rangle \tag{A.12}$$

$$\hat{n}(0) = \sum_{n} \langle n| \hat{n}(0)|n\rangle |n\rangle\langle n| \tag{A.13}$$

and by assuming that $\hat{n}(\tau)$ is diagonal in the form

$$\hat{n}(\tau) = \sum_{n} \langle n| \hat{n}(\tau)|n\rangle |n\rangle\langle n| \tag{A.14}$$

,we can infer from (A.10,A.11,A.12,A.13,A.14) that

$$\hat{n}(\tau) = \frac{A}{B} - \left[\frac{A}{B} - \hat{n}(0)\right]e^{-B\tau} \tag{A.15}$$

and hence the numerator of (A.2) equals

$$\langle 0| \hat{n}(\tau)|0\rangle = \frac{A}{B} - \left[\frac{A}{B} - 0\right]e^{-B\tau} = \frac{A}{B}\left(1 - e^{-B\tau}\right) \tag{A.16}$$

From (A.16), (A.2), (A.6) and (A.8) we can write

$$g^{(2)}(\tau) = \left(1 - e^{-B\tau}\right) \tag{A.17}$$

ACKNOWLEDGMENTS

Tarek Ahmed Mokhiemer, wants to thank King Fahd University of Petroleum and Minerals for hosting him as a graduate student doing the work presented in this paper in his masters thesis research, which owes much for the computing facilities in its Physics Department.

[1] Kyungwon An, James J. Childs, Ramachandra R. Dasari, and Michael S. Feld , Phys. Rev. Lett. 73, 3375 (1994)

[2] Maddox, John, The wonders of the Microlaser, Nature, Volume 373, Issue 6510, pp. 101 (1995)

[3] Wonshik Choi, Jai-Hyung Lee, Kyungwon An , C. Fang-Yen, R. R. Dasari, M. S. Feld, Phys. Rev. Lett. 96, 093603 (2006)

[4] McKeever, J., Boca, A., Boozer, A. D., Buck, J. R. and Kimble, H. J.

[5] Fam Le Kien, Georg M. Meyer, Ulrich W. Rathe, Marlan O. Scully, Herbert Walther, and Shi-Yao Zhu, Phys. Rev. A 52, 3279 (1995)

[6] A. Messina a; S. Maniscalco a; A. Napoli a, Journal of Modern Optics, Volume 50, Issue 1 January 2003 , pages 1 - 49

[7] Fam Le Kien, Georg M. Meyer, Marlan O. Scully, Herbert Walther, and Shi-Yao Zhu, Phys. Rev. A 49, 1367(1994)

[8] J. Dalibard, Y. Castin and K. M?lmer, Phys. Rev. Lett. 68, 580 (1992)

[9] R. Dum, A. S. Parkins, P. Zoller and C. W. Gardiner, Phys. Rev. A 46, 4382 (1992).

[10] J D Cresser and S M Pickles, Quantum Semiclass. Opt. 8, 73-104 (1996).

[11] H. J. Carmichael, An Open Systems Approach to Quantum Optics, Lecture Notes in Physics (Springer, Berlin , 1993).

[12] Marlan O. Scully and M. Suhail Zubairy, Quantum Optics, Cambridge University Press, 1997

[13] P. Meystre and M. Sargent III, Elements of Quantum Optics, 2nd Edition, Springer-Verlag, 1991

[14] Quang T., Phys. Rev. A, 46, 682 (1992)

[15] Weidinger, M.; Varcoe, B. T. H.; Heerlein, R.; Walther, H.,Phys. Rev. Lett., 82, 3975 (1999)

[16] Measurement of second order coherence in the Microlaser, Abdula-Aziz Aljalal, PhD Dissertation, 2001, MIT.

[17] P. Filipowicz, J. Javanainen, P. Meystre, Phys. Rev. A 34, 3077 (1986)

[18] R. Arun, G. S. Agarwal, M. O. Scully, and H. Walther, Phys. Rev. A, 62, 23809 (2000)